Finite Element Analysis of the Stress and Deformation Fields around the Blunting Crack Tip

Miresmaeili, Reza
Department of Intelligent Machinery and Systems, Graduate School of Engineering, Kyushu University

Ogino, Masao
Department of Mechanical Engineering, Faculty of Engineering, Kyushu University | AIST

Shioya, Ryuji
Department of Computational Science and Engineering, School of Engineering, Toyo University | AIST

Kawai, Hiroshi
Department of Systems Innovation, School of Engineering, University of Tokyo

他

出版情報：九州大学工学紀要. 68 (4), pp.151-161, 2008-12. Faculty of Engineering, Kyushu University
バージョン：
権利関係：

Memoirs of the Faculty of Engineering, Kyushu University, Vol.68, No.4, December 2008

Finite Element Analysis of the Stress and Deformation Fields around the Blunting Crack Tip

by

Reza MIRESMAEILI[*], Masao OGINO[**], Ryuji SHIOYA[***], Hiroshi KAWAI[†], and Hiroshi KANAYAMA[‡]

(Received September 2, 2008)

Abstract

The main object is to define the stress and deformation fields in a vicinity of a crack in an elasto-plastic power law hardening material under plane strain tensile loading. Hydrogen-enhanced localized plasticity (HELP) is recognized as an acceptable mechanism of hydrogen embrittlement and hydrogen-induced failure in materials. A possible way by which the HELP mechanism can bring about macroscopic material failure is through hydrogen-induced cracking. The distributions of the hydrostatic stress and plastic strain are simulated around the blunting hydrogen induced crack tip. The model of Sofronis and McMeeking is used in order to investigate the crack plasticity state. The approach is valid as long as small scale yielding conditions hold. Finite element analyses are employed to solve the boundary value problems of large strain elasto-plasticity in the vicinity of a blunting crack tip under mode I (tensile) plane-strain opening and small scale yielding conditions. Three different FEM softwares; MSC.Marc, ADVENTURE-Solid and ZeBuLoN are used for structural analysis and results are verified by the previous works. The aim is to compare the results of different rate equilibrium equations in the case of large deformation and large strain elasto-plastic analysis.

Keywords: Crack tip plasticity, Hydrogen-induced cracking, Hydrogen embrittlement, Small scale yielding conditions, Finite element

[*] Ph. D. Student, Department of Intelligent Machinery and Systems, Graduate School of Engineering, Kyushu University
[**] Assistant Professor, Department of Mechanical Engineering, Faculty of Engineering, Kyushu University and AIST
[***] Associate Professor, Department of Computational Science and Engineering, School of Engineering, Toyo University and AIST
[†] Research Associate, Department of Systems Innovation, School of Engineering, University of Tokyo
[‡] Professor, Department of Mechanical Engineering, Faculty of Engineering, Kyushu University and AIST

1. Introduction

Hydrogen embrittlement is a common type of failure. In presence of hydrogen, materials fail at a lower load levels in comparison to hydrogen-free materials. Hydrogen-enhanced localized plasticity (HELP) is an acceptable mechanism of hydrogen embrittlement and hydrogen-induced cracking in materials [1]. According to the HELP theory, the presence of hydrogen in a solid solution increases the dislocation motion, thereby increasing the amount of plastic deformation that occurs in a localized region adjacent to the fracture zone [2].

A possible way by which the HELP mechanism can bring about macroscopic material failure is through hydrogen-induced cracking. The fracture and fatigue behavior of a cracked plate under external load depends upon the stress and strain in the vicinity of the crack tip. Crack tip phenomena in hydrogen-induced cracking e.g. hydrogen concentration is often based upon the known details of the crack tip elasto-plastic state. When a body containing a crack is subject to a monotonically increasing load of the tensile opening mode, intense straining blunts the crack tip until some mechanism of crack extension either gradually or abruptly takes over [3]. McMeeking and Rice [4] presented a finite element formulation for problems of large elasto-plastic flow. According to their formulation, Sofronis and McMeeking [5] proposed a finite element model to show the effect of hydrostatic stress and trapping phenomenon on hydrogen distribution in plastically deformed steels. Based on their model Krom et al. [6] suggested a formulation to provide the correct balance of hydrogen into the considered material. Kanayama et al. [7] used a different finite element scheme from Krom et al. [6] and applied the Galerkin method in a 3D simulation in order to reconstruct the Sofronis and McMeeking's model [5]. Taha and Sofronis [8] reviewed the progress in analyzing the material mechanical behavior at a crack tip or a rounded notch with that of hydrogen diffusion. Kotake et al. [9] performed an unsteady hydrogen diffusion-elastoplastic coupling analysis near a blunting crack tip. According to their research, the hydrogen concentration near the crack tip depends greatly on the loading frequency.

The intent of this work is to solve a numerical formulation for crack tip analysis of the general plane strain problems. The hydrogen effects on the elasto-plastic behavior are not taken into consideration. The considered subject is the stress and deformation fields in a cracked elasto-plastic power law hardening material. Modeling has been done in three numerical softwares; ADVENTURE-Solid, MSC.Marc and ZeBuLoN, then the results are verified by the previous works. The aim is to validate the results of ADVENTURE-Solid software which was used by the authors in reference (7) and comparing the results of different rate equilibrium equations in the case of large deformation and large strain elasto-plastic analysis.

2. Formulation

The numerical formulation is an incremental plasticity finite element modeling specialized to crack analysis. The formulation has a general applicability and is used to solve the small scale yielding problems. The applied formulation in an elasto-plastic isotropic hardening material satisfies the von-Mises yield criterion**.**

$$3\sigma'_{ij}\sigma'_{ij}/2-\bar{\sigma}_y^2=0\,, \tag{1}$$

σ'_{ij} represents the deviatoric stress tensor (which is calculated by the formulation explained in the next section) and the flow stress is $\bar{\sigma}_y$. A power law hardening rule is used; that is, the flow stress

is considered to be a function of the equivalent plastic strain $\bar{\varepsilon}^p$.

$$\left(\frac{\bar{\sigma}_y}{\sigma_0}\right)^{1/N} = \frac{\bar{\sigma}_y}{\sigma_0} + \frac{3G}{\sigma_0}\bar{\varepsilon}^p, \tag{2}$$

where σ_0 is the initial yield stress, G is shear modulus and N is the work hardening exponent. Here $\bar{\varepsilon}^p$ is defined in terms of the plastic strain tensor ε_{ij}^p as

$$\bar{\varepsilon}^p = \left(2\varepsilon_{ij}^p\ \varepsilon_{ij}^p / 3\right)^{1/2}. \tag{3}$$

2.1 Rate equilibrium equations

To find the solution of the rate equations in the total Lagrangian approach, the initial distribution of stress, the initial configuration of the body and the initial values of material properties are supposed to have already been determined. The aim is to calculate the internal velocity field when the rates of change of the surface loads, body forces and geometrical constraints are prescribed.

To solve the proposed boundary value problems, the second Piola-Kirchhoff stress S_{ij} is defined associated with the corresponding coordinates where the initial position of elements is specified by rectangular Cartesian co-ordinate X_i. b_i^0 is the elementary (body) force on a volume element per unit initial volume, therefore; continuum equilibrium equation under body-force per unit initial volume is

$$\frac{\partial S_{ij}}{\partial X_j} + b_i^0 = 0. \tag{4}$$

The change of the traction on an element with an initial unit normal n_j has components

$$f_i^0 = n_j\ S_{ij}. \tag{5}$$

The body-force is given in the initial volume V^0 while the nominal traction f_i^0 is prescribed on a part S_f^0 of the initial surface S^0. As essential boundary conditions, the virtual displacements η_i vanishes on the remainder surface $S^0 - S_f^0$; therefore, a formulation of equilibrium can be expressed by the principle of virtual work as Eq. (6).

$$\int_{V^0} S_{ij}\ \delta E_{ij}\ dV^0 = \int_{S_f^0} f_i^0\ \delta\eta_i\ dS^0 + \int_{V^0} b_i^0\ \delta\eta_i\ dV^0, \tag{6}$$

where E_{ij} is the Green-Lagrange strain. Integrations are carried out in the original configuration.

For viscoelastic fluids and elasto-plastic and viscoplastic solids, the constitutive equations usually supply an expression for the rate of stress in terms of deformation rate, stress, deformation, and sometimes other (internal) material parameters. The relevant quantity for the constitutive

equations is the rate of stress at a given material point.

Based on Hill's paper [10], McMeeking and Rice [4] used a concise formulation of rate equilibrium at arbitrary amounts of deformation given by the following form of the virtual work equation.

$$\int_{V^0} \dot{t}_{ij} \left(\frac{\partial(\delta \upsilon_j)}{\partial X_i} \right) dV^0 = \int_{S_f^0} \dot{f}_j^0 \, \delta \upsilon_j \, dS^0 + \int_{V^0} \dot{b}_j^0 \, \delta \upsilon_j \, dV^0 , \tag{7}$$

where all integration extents are in the reference configuration and X_i is the position vector of a material point in that reference state. t_{ij} is the non-symmetric nominal stress. $\delta \upsilon_j$ is an arbitrary virtual velocity variation which disappears on $S^0 - S_f^0$ where the velocity rates are prescribed. (Note that rates are indicated by the superposed dot). In order to use the updated Lagrangian formulation, Eq. (7) should be rewritten in current configuration. Note that $\dot{t}_{ij}$ is not symmetric and does not vanish in a rigid body spin; therefore, it may be simply related to spin-invariant stress rate, Jaumann rate of Kirchhoff stress, more suitable to be used in constitutive relations. According to Hill [10], the nominal stress t is simply related to Kirchhoff stress having components t_{ij} and τ_{ij} respectively.

$$\dot{t}_{ij} = \dot{\tau}_{ij} + \tau_{ik} \upsilon_{j,k} . \tag{8}$$

The Jaumann rate of Kirchhoff stress is given by

$$\overset{\circ}{\tau}_{ij} = \dot{\tau}_{ij} - W_{ik} \tau_{kj} + \tau_{ik} W_{kj} . \tag{9}$$

where $W_{ij} = \frac{1}{2}\left(\upsilon_{i,j} - \upsilon_{j,i} \right)$ is the spin tensor.

Instead of the co-rotational stress rate $\overset{\circ}{\tau}$, one can use the convected stress rate [11].

$$\overset{*}{\tau}_{ij} = \overset{\circ}{\tau}_{ij} + D_{ik} \tau_{kj} + \tau_{ik} D_{kj} = \dot{\tau}_{ij} + \upsilon_{k,i} \tau_{kj} + \tau_{ik} \upsilon_{k,j} , \tag{10}$$

where $D_{ij} = \frac{1}{2}\left(\upsilon_{i,j} + \upsilon_{j,i} \right)$ is the rate of deformation or stretching tensor.

By substituting Eq. (10) in Eq. (8) and considering the symmetry part of the deformation velocity (i.e. $W = 0$)

$$\dot{t}_{ij} = \overset{*}{\tau}_{ij} - \tau_{kj} D_{ki} - \tau_{ik} D_{kj} + \tau_{ik} \upsilon_{j,k} , \tag{11}$$

where the Kirchhoff stress $\tau = J \sigma$. J is the ratio of volume in the reference state to volume in the current state and σ is the Cauchy stress. When the reference configuration is taken at the

instant under consideration, then $J=I$ [10].

By this assumption, Eq. (11) is rewritten as

$$\dot{t}_{ij} = \overset{*}{\tau}_{ij} - \sigma_{kj} D_{ki} - \sigma_{ik} D_{kj} + \sigma_{ik} \upsilon_{j,k} . \tag{12}$$

Under these conditions, Eq. (7) becomes

$$\int_V \left[\overset{*}{\tau}_{ij} \, \delta D_{ij} - \frac{1}{2} \sigma_{ij} \delta \left(2 D_{ik} D_{kj} - \upsilon_{k,i} \, \upsilon_{k,j} \right) \right] dV = \int_S \dot{f}_j^0 \delta \upsilon_j dS + \int_V \dot{b}_j^0 \delta \upsilon_j dV , \tag{13}$$

where all integration extents are in the current configuration. $\dot{b}_j^0$ and $\dot{f}_j^0$ are still nominal force intensity rates. This formulation was used by Sofronis and McMeeking [5] for structural analysis. In the Eq. (13), $\overset{*}{\tau}$ is the convected stress rate while in the reference [5] the co-rotational stress rate $\overset{\circ}{\tau}$ is used.

Another way to get the rate formulation is to differentiate the Lagrangian virtual work equation i.e. Eq. (6) with respect to time. The rate of virtual work is readily found as Eq. (14):

$$\int_{V^0} \left[\dot{S}_{ij} \, \delta E_{ij} + S_{ij} \frac{\partial \upsilon_k}{\partial X_j} \frac{\partial \delta \eta_k}{\partial X_i} \right] dV^0 = \int_{S_f^0} \dot{f}_i^0 \, \delta \eta_i \, dS^0 + \int_{V^0} \dot{b}_i^0 \, \delta \eta_i \, dV^0 . \tag{14}$$

We wish to use the updated Lagrangian formulation so that we now transform Eq. (14) to an equation referring to the current configuration. Keeping in view that the reference state is the current state, a rate formulation similar to Eq. (14) can be obtained by setting

$$\delta E_{ij} = \delta D_{ij} , \quad \frac{\partial}{\partial X_i} = \frac{\partial}{\partial x_i} , \quad S_{ij} = \sigma_{ij} , \tag{15}$$

Hence,

$$\int_V \left[\overset{\nabla}{\sigma}_{ij} \, \delta D_{ij} + \sigma_{ij} \frac{\partial \upsilon_k}{\partial x_j} \frac{\partial \delta \eta_k}{\partial x_i} \right] dV = \int_S \dot{f}_i \, \delta \eta_i \, dS + \int_V \dot{b}_i \, \delta \eta_i \, dV \tag{16}$$

in which b_i and f_i are the body force and surface traction, respectively, in the current configuration. In this equation, $\overset{\nabla}{\sigma}_{ij}$ is the Truesdell rate of the Cauchy stress [12]. The following is the well known expression [12] for the Truesdell rate of the Cauchy stress:

$$\overset{\nabla}{\sigma}_{ij} = \dot{\sigma}_{ij} - \sigma_{ik} \upsilon_{j,k} - \sigma_{kj} \upsilon_{i,k} + \sigma_{ij} \upsilon_{k,k} . \tag{17}$$

The Truesdell rate of the Cauchy stress is materially objective (frame indifferent). If a rigid body motion is imposed on the material, the Truesdell rate vanishes, whereas the usual material rate does not vanish. Constitutive variational statements of Eqs. (13) and (16) is cited in the current paper and integrated by the backward Euler method, respectively, in ADVENTURE-Solid and MSC.Marc[13]. The constitutive equations can be formulated in terms of the Jaumann rate of Kirchhoff stress [4] or Truesdell rate of the Cauchy stress as

$$\overset{\nabla}{\sigma}_{ij} = L_{ijkl} \, D_{kl} , \tag{18}$$

and

$$L_{ijkl} = \frac{1}{J} F_{im} F_{jn} F_{kp} F_{lq} D_{mnpq}\,, \tag{19}$$

in which D_{mnpq} represents the material moduli tensor in the reference configuration which is convected to the current configuration with material moduli tensor L_{ijkl}.

3. The elasto-plastic boundary value problems at a blunting crack tip

The numerical finite element analyses are employed to solve the boundary value problems of large strain elasto-plasticity in the vicinity of a blunting crack tip under mode I (tensile) plane-strain opening and small scale yielding conditions. Small scale yielding refers to the situation when plasticity is so localized at the crack tip that the elastic dominant singular solution holds at a remote distance from the yield zone [14]. **Figure 1** shows the half-symmetry geometry domain and the finite element mesh defined for the analysis in ZeBuLoN and Msc.Marc softwares. The elements increase in size in the radial direction by a growth factor of 1.1. The used element type in ZeBuLoN [15] is 2D continuum quadrilateral elements with reduced integration in order to simulate the incompressibility of material behavior whereas MSC.Marc [16] has plane strain eight-node distorted quadrilateral elements with reduced integration Herrmann formulation for this purpose.

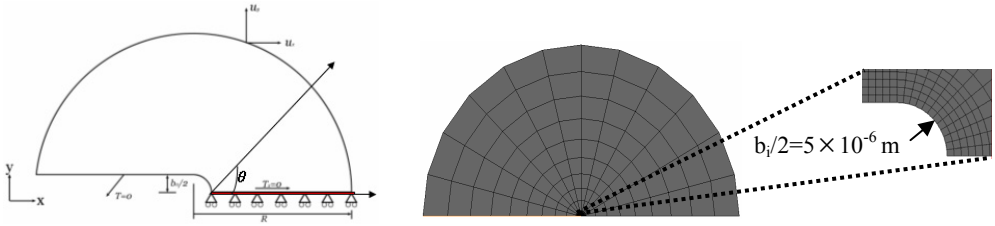

(a) (b) (c)

Initial crack opening displacement (b_i) $=1\times10^{-5}$ m

Radius of the half-symmetry domain (R)=0.15 m

Thickness of the elements in the plane strain analysis (t)= 8.25×10^{-4} m

Fig. 1 (a) Geometry of the model and boundary conditions; (b) small –scale yielding mesh; (c) mesh configuration in vicinity of the crack tip.

Figure 2 illustrates the three dimensional mesh with 3,706 nodes and 1,776 8-node hexahedral elements which is used in ADVENTURE-Solid [17]. As can be seen in the figure, the mesh is refined near the crack tip. Authors used the result of ADVENTURE-Solid software which is concluded by using a reduced (selective) integration technique in order to model the effect of elasto-plastic state at the crack-tip on hydrogen diffusion problems [7]. Plane strain local yielding situations are considered and the constitutive variational statement of Eq. (13) and (16) were integrated by the backward Euler method, respectively, in ADVENTURE-Solid [17] and MSC.Marc [13] software. The yielded zone is confined to a small region near the crack tip that is negligible in size in comparison to geometric dimension such as crack length, un-cracked specimen width, etc. In this situation according to reference (18), we employ a special boundary layer type formulation of the problems. The actual configuration is then replaced by the simpler semi-infinite body, and a boundary layer

approach is employed replacing actual boundary conditions in **Fig.3** with the asymptotic boundary conditions as Eqs. (20) and (21).

$$u_x(R,\theta)=K_I\frac{1+\nu}{E}\sqrt{\frac{R}{2\pi}}\cos\left(\frac{\theta}{2}\right)(3-4\nu-\cos\theta), \tag{20}$$

$$u_y(R,\theta)=K_I\frac{1+\nu}{E}\sqrt{\frac{R}{2\pi}}\sin\left(\frac{\theta}{2}\right)(3-4\nu-\cos\theta), \tag{21}$$

where K_I is the stress intensity factor from the linear elastic crack solution. E and ν are, respectively, Young's modulus and Poisson ratio of the material and θ is the polar angle as shown in **Fig.3**.

Symmetry boundary conditions are applied on the crack plane y=0. The symmetry line $\theta=0$ is free of shear tractions and displacements in the y direction (see **Figs. 1** and **3**). The load is increasing from zero at a rate of 0.69 MPa(m)$^{0.5}$s^{-1} for 130 s with steps of 0.5 s. At 130 s the crack tip opening displacement b_c, according to Tracey [14], is 4.7 times the initial crack tip opening displacement b_i. The finite element computations using the updated Lagrangian formulation with the full Newton-Raphson method are performed by three softwares; ADVENTURE-Solid, MSC.Marc and ZeBuLoN.

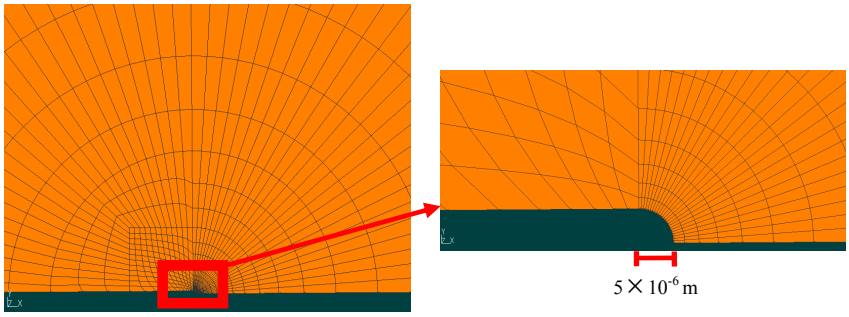

Fig. 2 Refined mesh used in ADVENTURE-Solid in the vicinity of the crack tip (thickness=8.25×10^{-4} m).

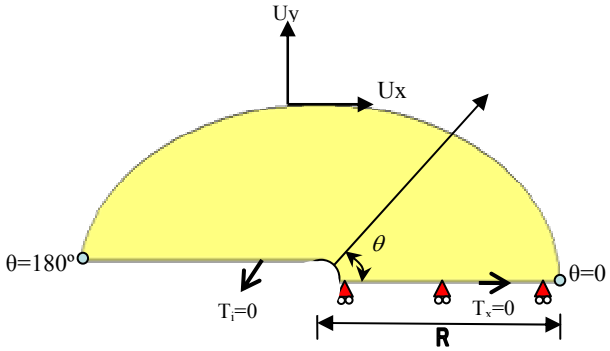

Fig. 3 Boundary conditions of small scale yielding approach for a half-symmetry domain with the radius of R=0.15 m.

4. Numerical results and discussions

The material used in the simulation is the BCC impure iron whose properties are given in **Table 1**.

Table1 Material properties of BCC impure iron.

Properties	Symbol	Value
Young's modulus	E	$207\times10^{+9}$ N/m^2
Poisson ratio	ν	0.3
Initial yield stress	σ_0	$250\times10^{+6}$ N/m^2
Work hardening exponent	N	0.2

The displacement contours in x direction concluded from MSC. Marc and ZeBuLoN are shown in **Fig.4** for comparison. Not only is there a good agreement between the shapes of the contours but also the maximum displacement concluded from two mentioned FEM softwares are almost the same (i.e. U_x=1.104×10^{-4} m for MSC. Marc and U_x=1.110×10^{-4} m for ZeBuLoN).

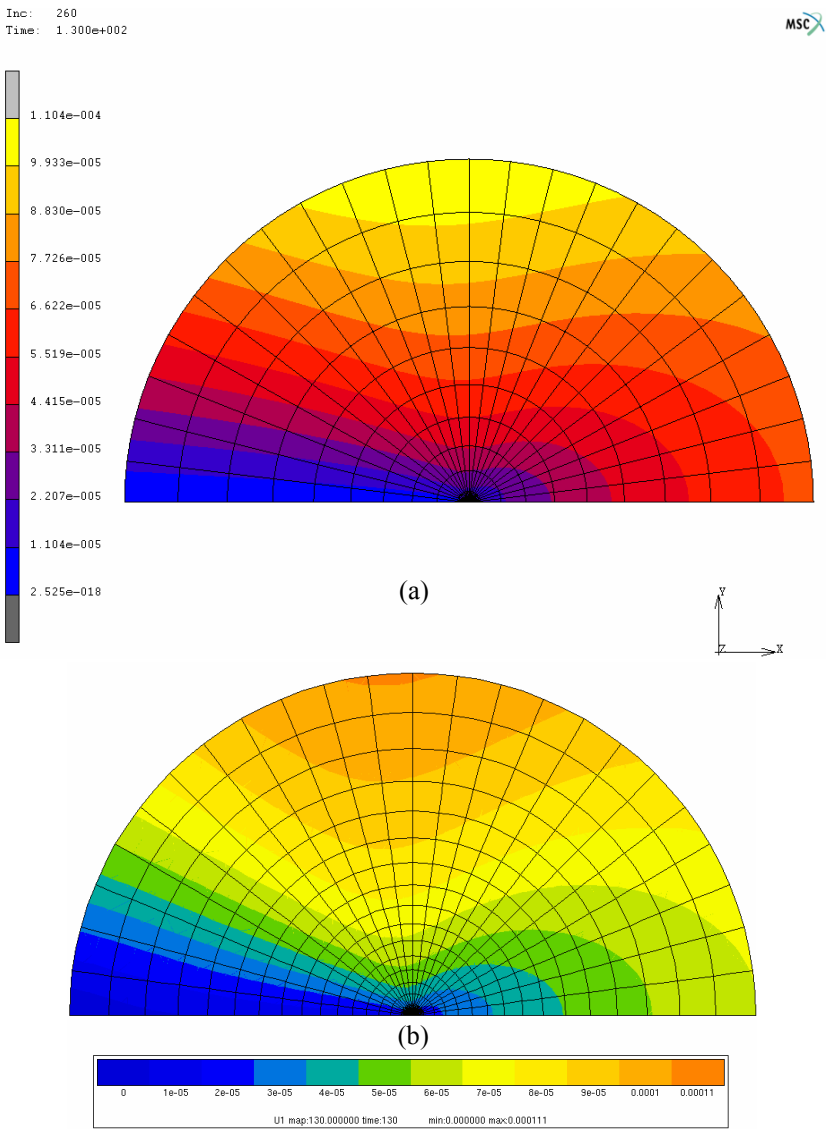

Fig. 4 Displacement in x direction concluded from; (a) MSC. Marc and (b) ZeBuLoN.

In **Fig.5** the equivalent plastic strain $\bar{\varepsilon}^p$ produced at 130 s plotted against the distance of the initial position of each node from the notch root (X) normalized by b_c i.e. crack opening displacement after 130 s in the undeformed configuration for $\theta = 0$ is compared with the result of Sofronis and McMeeking[5] for ADVENTURE-Solid and MSC. Marc. The comparison between the current analysis and the previous one represents satisfying results (see **Fig.5**). Incompressibility of material behavior was enforced by the method of selective (or reduced) integration as explained in section 3.

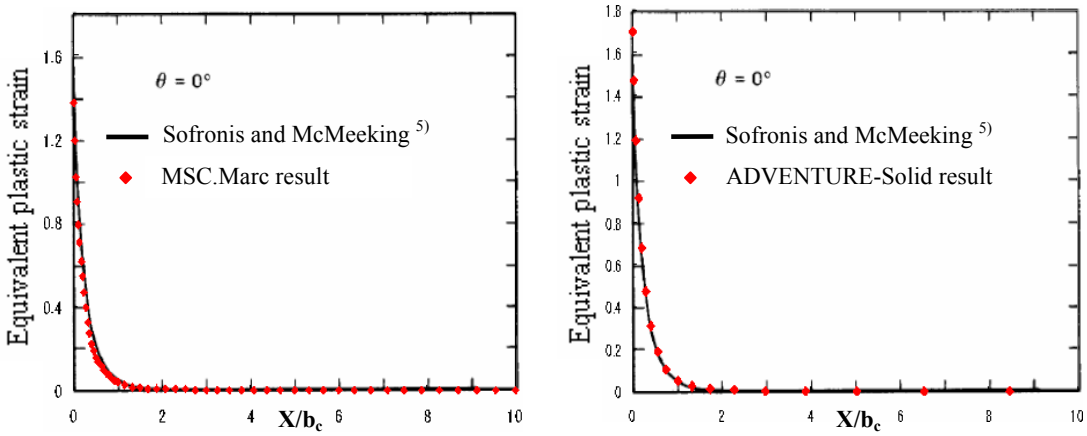

Fig. 5 Plot of equivalent plastic strain $\bar{\varepsilon}^p$ vs distance X/b_c after 130 s when the crack opening displacement b_c is equal to $4.7b_i$ (X is the distance of the initial position of each node from the notch root in the undeformed configuration); (a) MSC.Marc, (b) ADVENTURE-Solid.

Figure 6 illustrates the equivalent von-Mises stress around the vicinity of the crack tip. As can be seen in this figure, there is a significant gradient of von-Mises stress near the crack tip.

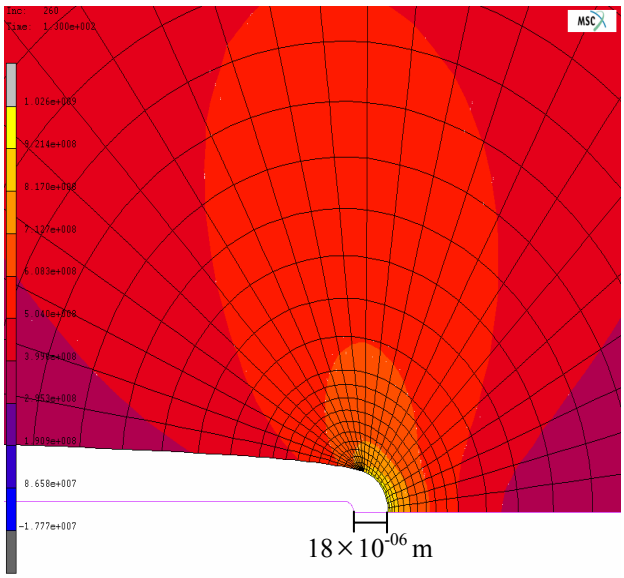

Fig. 6 Contour of equivalent von-Mises stress near the crack tip.

Figure 7 illustrates the hydrostatic stress in the vicinity of the crack tip on symmetry line i.e. $\theta = 0$ after 130 s. In this figure, the results of ADVENTURE- Solid and ZeBuLoN analyses have been compared with Sofronis and Mc.Meeking [5] and Krom et al. [6]. As can be seen the maximum of hydrostatic stress is located at a position close to the crack root in the undeformed configuration (X/b_c=1.75).

5. Conclusion

Structural finite element analyses were implemented in order to investigate the distribution of hydrostatic stress and equivalent plastic strain in the vicinity of a blunting hydrogen-induced crack tip. The displacement and hydrostatic stress distributions obtained in ADVENTURE-Solid, MSC.Marc and ZeBuLoN by using different rate equilibrium equations as explained in this paper were verified by the results of Sofronis and McMeeking's study [5] and Krom et al. [6]. In each case there is a good agreement between the results so it shows that the numerical model of Sofronis and McMeeking's paper [5] has been reconstructed successfully and the mentioned model produces considerably same results by different rate equilibrium equations. Following this study, by using the results of ADVENTURE-Solid, authors have already published a paper explaining an analysis in order to determine the hydrogen distribution around the crack tip using the boundary value approach[7]. The next study will be the fully coupled analysis in order to investigate the effect of hydrogen concentration on softening of materials as well as hydrogen distribution analysis around the crack tip.

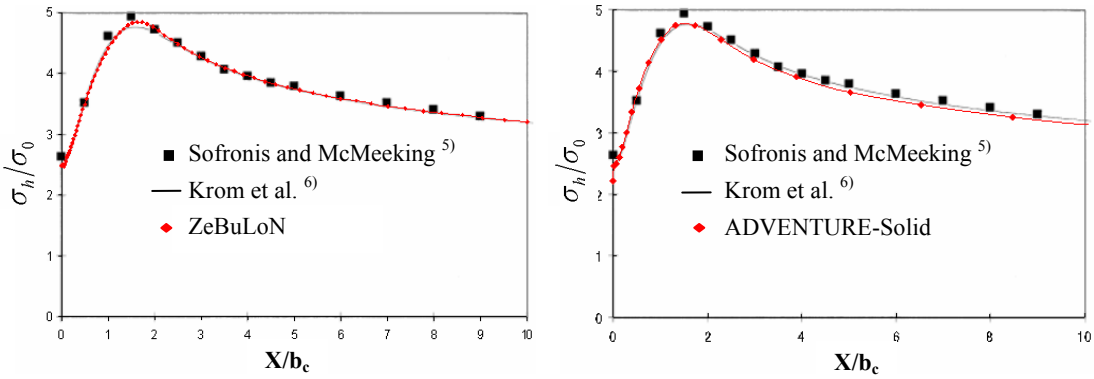

Fig. 7 Plot of normalized hydrostatic stress vs distance X/b_c after 130 s when the crack opening displacement b_c is equal to $4.7b_i$ (X is the distance of the initial position of each node from the notch root in the undeformed configuration); (a) ZeBuLoN, (b) ADVENTURE-Solid.

Acknowledgments

This research has been conducted as a part of "Fundamental Research Project on Advanced Hydrogen Science" funded by New Energy and Industrial Technology Development Organization (NEDO). The authors gratefully acknowledge the assistance of Prof. J. M. Olive, Dr. N. Saintier and Mr. A. Lavoil in performing the analysis in ZeBuLoN software.

References

1)Meyers, S. M. et al., Hydrogen interactions with defects in crystalline solids, *Reviews of Modern Physics*, Vol. 64, No. 2, pp. 559–617 (1992).
2)Tabata, T., Birnbaum H. K., Direct observations of the effect of hydrogen on the behavior of dislocations in iron, *Scripta Metallurgica*, Vol. 17, pp. 947-950 (1983).
3)McMeeking, R. M., Finite deformation analysis of crack-tip opening in elastic-plastic materials and implications for fracture, *Journal of the Mechanics and Physics of Solids*, Vol. 25, pp. 357-381 (1997).
4)McMeeking, R. M., Rice, J. R., Finite-element formulations for problems of large elastic-plastic deformation, *International Journal of Solids and Structures*, Vol. 11, No. 5-F, pp. 601-616 (1975).
5)Sofronis, P., McMeeking, R. M., Numerical analysis of hydrogen transport near a blunting crack tip, *Journal of the Mechanics and Physics of Solids*, Vol. 37, No.3, pp. 317-350 (1989).
6)Krom, A. H. M., Koers, R. W. J., Bakker, A., Hydrogen transport near a blunting crack tip, *Journal of the Mechanics and Physics of solids*, Vol. 47, pp. 971-992 (1999).
7)Kanayama, H., Shingoh, T., Ndong-Mefane, S., Ogino, M., Shioya, R., Kawai, H., Numerical analysis of hydrogen diffusion problems using the finite element method, *Theoretical and Applied Mechanics Japan*, Vol. 56, pp. 389-400 (2008).
8)Taha, A., Sofronis, P., A micromechanics approach to the study of hydrogen transport and embrittlement, *Engineering Fracture Mechanics*, Vol. 68, pp. 803-837 (2001).
9)Kotake, H., Matsumoto, R., Taketomi, S., Miyazaki, N., Transient hydrogen diffusion analyses coupled with crack-tip plasticity under cyclic loading, *International Journal of Pressure Vessels and Piping*, Vol. 85, pp. 540–549 (2008).
10)Hill, R., Some basic principles in the mechanics of solids without a natural time, *Journal of the Mechanics and Physics of Solids*, Vol. 7, pp. 209-225 (1959).
11)Truesdell, C., Noll, W., The nonlinear field theories of mechanics. In: Flugge S., editor, *Handbuch der Physik*, Vol. III, Berlin, Springer, p. 404 (1965).
12)Truesdell, C., The simplest rate theory of pure elasticity, *Communications on pure and applied mathematics*, Vol. 8, pp. 123-132 (1955).
13)MSC.Marc 2005 r3 Help Manual, *MSC.Marc Volume A: Theory and User Information*, User Documentation: Copyright © 2006 MSC.Software Corporation, Printed in U.S.A., pp. 131-141.
14)Tracey, D. M., Finite element solutions for crack-tip behavior in small-scale yielding, *Journal of Engineering Materials and Technology*, Vol. 98, pp. 146-151 (1976).
15)Handbook of Z-set Version 8.4, *Release Notes Zmaster*, Transvalor / ENSMP Centre des Mat´eriaux & Northwest Numerics, March, pp. 6.4-6.5 (2006).
16)MSC.Marc 2005 r3 Help Manual, *MSC.Marc Volume B: Element Library*, User Documentation: Copyright © 2006 MSC.Software Corporation, Printed in U.S.A., pp. 368-372.
17)Yoshimura, S., Shioya, R., Noguchi, H., and Miyamura, T., Advanced general-purpose computational mechanics system for large-scale analysis and design, *Journal of Computational and Applied Mathematics*, Vol.149, pp. 279-296 (2002).
18)Rice, J. R., A path independent integral and the approximate analysis of strain concentration by notches and cracks, *Report E39*, Division of Engineering, Brown University Providence, May (1967).